Seed-Mediated Synthesis and Photoelectric Properties of Selenium Doped Zinc Oxide Nanorods
(Sintesis Bermediasi Benih dan Sifat Fotoelektrik Selenium Terdop Nanorod Zink Oksida)

Ari Sulistyo Rini*, Yolanda Rati, Miranti Agustin, Yanuar Hamzah & Akrajas Ali Umar

ABSTRACT

Pristine ZnO and selenium doped ZnO (Se-ZnO) nanorods were successfully synthesized using seed-mediated hydrothermal method. The growth solution of both pure and Se-doped ZnO nanorods employed zinc nitrate hexahydrate (ZNH) and hexamethylenetetramine (HMT) as a precursor and surfactant, respectively. As a dopant source, selenium salt solution was obtained by reacting selenium powder with sodium borohydride at low temperature. The as-prepared pure ZnO and Se-doped ZnO nanorods were characterized using field effect scanning electron microscopy (FESEM), X-ray diffraction (XRD), UV-Visible spectroscopy (UV-Vis), and Photoluminescence (PL) spectroscopy. FESEM images show that the geometric shape of Se-ZnO nanoparticles is nanorods with a hexagonal cross-section. The XRD pattern shows the diffraction peak of the sample at the angles of 2θ: 34.44°, 36.25° and 47.54° which represents the hkl plane of (002), (101) and (102), respectively. The crystalline size calculated from XRD data is found to be in the range of 35-42 nm. The UV-Vis spectrum shows that Se-ZnO nanorods strong absorption peaks appeared in the range of 300-380 nm for all samples. Se doping has slightly altered the band gap energy of pure ZnO nanorods around 0.01 eV. The peak of the photoluminescence spectra of the sample at 470 nm indicates the blue emission band.

Keywords: FESEM; PL spectra; selenium doping; UV-Vis; XRD; zinc oxide

ABSTRAK

ZnO asli dan selenium terdop nanorod ZnO (Se-ZnO) berjaya disintesis menggunakan kaedah hidroterma biji benih. Larutan pertumbuhan bagi kedua-dua ZnO asli dan Se-ZnO adalah menggunakan zink nitrat heksahidrat (ZNH) dan hexametilenetetramina (HMT) masing-masing sebagai pelopor dan surfaktan. Sebagai sumber pengedopan, larutan garam selenium diperoleh daripada tindak balas serbuk selenium dengan natrium borohidrida pada suhu rendah. ZnO asli dan Se-ZnO dicirikan menggunakan mikroskopi elektron imbasan pancaran medan (FESEM), pembelauan sinar-X (XRD), spektroskopi UV (UV-Vis) dan spektroskopi fotoluminesen (PL). Imej FESEM menunjukkan bentuk geometri nanozarah Se-ZnO adalah nanorod dengan keratan rentas heksagon. Corak XRD pula menunjukkan puncak belauan sampel pada sudut 2θ: 34.44°, 36.25° dan 47.54° yang mewakili satah hkl masing-masing pada (002), (101) dan (102). Saiz kristal yang dihitung daripada data XRD berada dalam julat 35-42 nm. Spektrum UV-Vis menunjukkan bahawa puncak penyerapan nanorod Se-ZnO muncul pada julat 300-380 nm untuk semua sampel. Pengedopan Se mengubah sedikit tenaga jurang jalur nanorod ZnO tulen sekitar 0.01 eV. Puncak spektra fotoluminesen pula muncul pada 470 nm menunjukkan jalur pancaran biru.

Kata kunci: FESEM; pengedopan selenium; spektra PL; UV-Vis; XRD; zink oksida

INTRODUCTION

ZnO (Zinc Oxide) is a II-VI group semiconductor that possesses wide band gap (3.37 eV) and large exciton binding energy (60 MeV) with high photosensitivity, piezoelectric, and pyroelectric properties (Janotti & Van De Walle 2009). ZnO, with the exciton binding energy of 60 MeV, might efficiently produce electron emission in ultraviolet range (< 400 nm) at room temperature. These properties have made ZnO applicable in several devices such as solar cells (Luo et al. 2018), LEDs (Light-Emitting Devices), gas sensors (Zhu & Zeng 2017), biosensors (Karim et al. 2019), piezoelectric transducers (Zakaria et al. 2017), and pyroelectric devices (Tan et al. 2009). ZnO is a versatile material that can substitute TiO_2 in several application because ZnO has good transparency and higher electron mobility (Rong et al. 2019). In addition, ZnO has low defects (Thangavel & Chang 2012), and can be easily

fabricated in various nanostructures at low temperature (Singh 2013). In order to enhance the properties of ZnO, ZnO is normally doped with different impurities to develop fascinating characteristics. This is accomplished by creating the desired properties and functions, including altering the band structure, establishing defect sites and promoting the mobility of charge carriers (Taha et al. 2019). In many application such as solar cells, catalyst and sensors, it is essential to adjust the electrical, optical and magnetic properties of ZnO (Chen et al. 2017; Nenavathu et al. 2018).

ZnO is commonly doped by various impurity such as metal In (Abrar et al. 2012), B (Rahman et al. 2016), Mg (Corral-Aguado et al. 2016), Mn (Achouri et al. 2016), Ni (Yilmaz et al. 2012), Al (Thu & Maenosono 2010), Ga (Alexandrov et al. 2020), Li (Alexandrov et al. 2020) or nonmetal N (Bangbai et al. 2013), C (Alshammari et al. 2015), S (Wang et al. 2013), and Se (Taha et al. 2019). Doping of ZnO with nonmetals might affect the band gap and the photoelectronic properties of undoped ZnO nanoparticles (Chen et al. 2008). Selenium (Se) was selected because of its excellent chemical properties (Chen et al. 2017). In addition, the high reduction potential of Se is a desirable condition for the extraction of photo-excited electrons from the conduction band (CB) and can therefore promote the production of reactive oxygen species (Nenavathu et al. 2018).

ZnO doping with Se has enhanced photoelectrochemical and photocatalytic properties of ZnO (Chen et al. 2017). Se-doped ZnO (Se-ZnO) NPs has previously been synthesized using thermomechanical methods (Nenavathu et al. 2018), photoelectrochemistry (Chen et al. 2017), chemical vapor transportation methods (Kumar et al. 2002), and sol-gel methods (Mustafa et al. 2018). However, these methods need complicated devices and are conducted at high temperature. In this work, the undoped and Se-doped ZnO nanorods were synthesized using a seed-mediated hydrothermal method at low temperatures. Doping of ZnO with low addition of Se was rarely studied. In this report, Se-doped ZnO nanorods was prepared by adding 0.025, 0.05, 0.1, and 0.2 mL of Se salt solution into the growth solution. Characterizations involved in this study were field effect scanning electron microscope (FESEM), X-ray diffraction (XRD), ultraviolet-visible absorption spectroscopy (UV-Vis), and photoluminescence (PL).

MATERIAL AND METHODS

MATERIAL

Zinc acetate dihydrate $Zn(CH_3COO)_2.2H_2O$ ($\geq$ 99.0% ACS Reagent) hexamethylenetetramine (HMT) $(CH_2)_6N_4$ (> 99.0% ACS Reagent) and Fluorine-doped Tin Oxide (FTO) glasses were purchased from Sigma Aldrich. Zinc nitrate hexahydrate, $Zn(NO_3)_2.6H_2O$ (Analytical Reagent) and Se powder were obtained from R&M Chemicals. Absolute ethanol C_2H_5OH (99%) and acetone (~97%) were provided by HmbG® Chemicals. Deionized water was obtained from Millipore water system.

SYNTHESIS OF ZNO AND SE-ZNO NANORODS

The pristine ZnO and Se-ZnO nanorods were grown on an FTO substrate using seed-mediated hydrothermal methods. Previously, the FTO substrate was subsequently cleaned by distilled water, acetone, and ethanol for 15 min using an ultrasonic bath. ZnO seeds solution was made by dissolving 22 mg of zinc acetate dihydrate into 10 mL of absolute ethanol. The solution was dropped on the FTO substrate and then spin-coated with a rotation speed of 3000 rpm for the 30 s. The sample was heated using a hotplate at 100 °C for 15 min. The coating process was repeated 3 times to get uniform ZnO seed.

ZnO growth solution was prepared by dissolving equimolar 10 mM zinc nitrate hexahydrate and 10 mM hexamethylenetetramine. As a dopant source, selenium salt solution was previously prepared by reacting selenium powder with 100 mM sodium borohydride at low temperature. Doping concentration was controlled by varying the selenium salt solution volumes in the growth solution (0.025, 0.05, 0.1, and 0.2 mL). Those samples were named according to their selenium solution volume (ZnO+Se 0.025 mL, ZnO+Se 0.05 mL, ZnO+Se0.1 mL, and ZnO+Se 0.2 mL). ZnO seeds films were then vertically immersed in the growth solution and heated at 90 °C for 5 h. After the growth process is completed, the sample is taken out from the solution and then cleaned with a copious amount of deionized water.

MATERIAL CHARACTERIZATION

The morphology of the samples was obtained using field emission scanning electron microscope (FESEM, ZEISS MERLIN type, Compact Co. Ltd.). The crystal structure was determined by X-ray diffraction (XRD, using a BRUKER EIXS type diffractometer). The UV-Vis spectrophotometer HITACHI U-3900H was used to characterize the UV-Vis diffuse reflectance spectra of the samples. The fluorescence measurements of the obtained films were performed in and FLS920 photoluminescence spectrometers (Edinburgh instruments).

RESULTS AND DISCUSSION

SURFACE MORPHOLOGY

The FESEM of ZnO-pure and Se-ZnO nanorod synthesized using the seed. The FESEM image of undoped and Se-doped ZnO samples indicated the morphology of nanorod with hexagonal cross-section. Figure 1(B), 1(D), 1(F), 1(H), 1(J) shows the particle size distribution of ZnO nanorods grown on the substrate. It is clearly seen that ZnO

nanorod grows more evenly and more densely after the addition of Se elements into the ZnO compounds. Based on the histogram graph in Figure 1, the mean rods diameter of the samples tends to increase. The rods diameter of pristine ZnO sample are 46.89 ± 15.9 nm, while the rod diameter of Se-doped ZnO sample are increased up to 64.68 ± 18.0 nm. An increase in nanorod size might be due to the ionic radius of Se^{2-} (190 pm) larger than that of O^{2-} (140 pm) which influence the molecule size of Se-ZnO mediated hydrothermal method are shown in Figure 1. The FESEM image was captured with 30,000 times of magnification. Particle size distribution (nanorod diameter) of the ZnO pure and Se-doped ZnO samples are presented in Table 1.
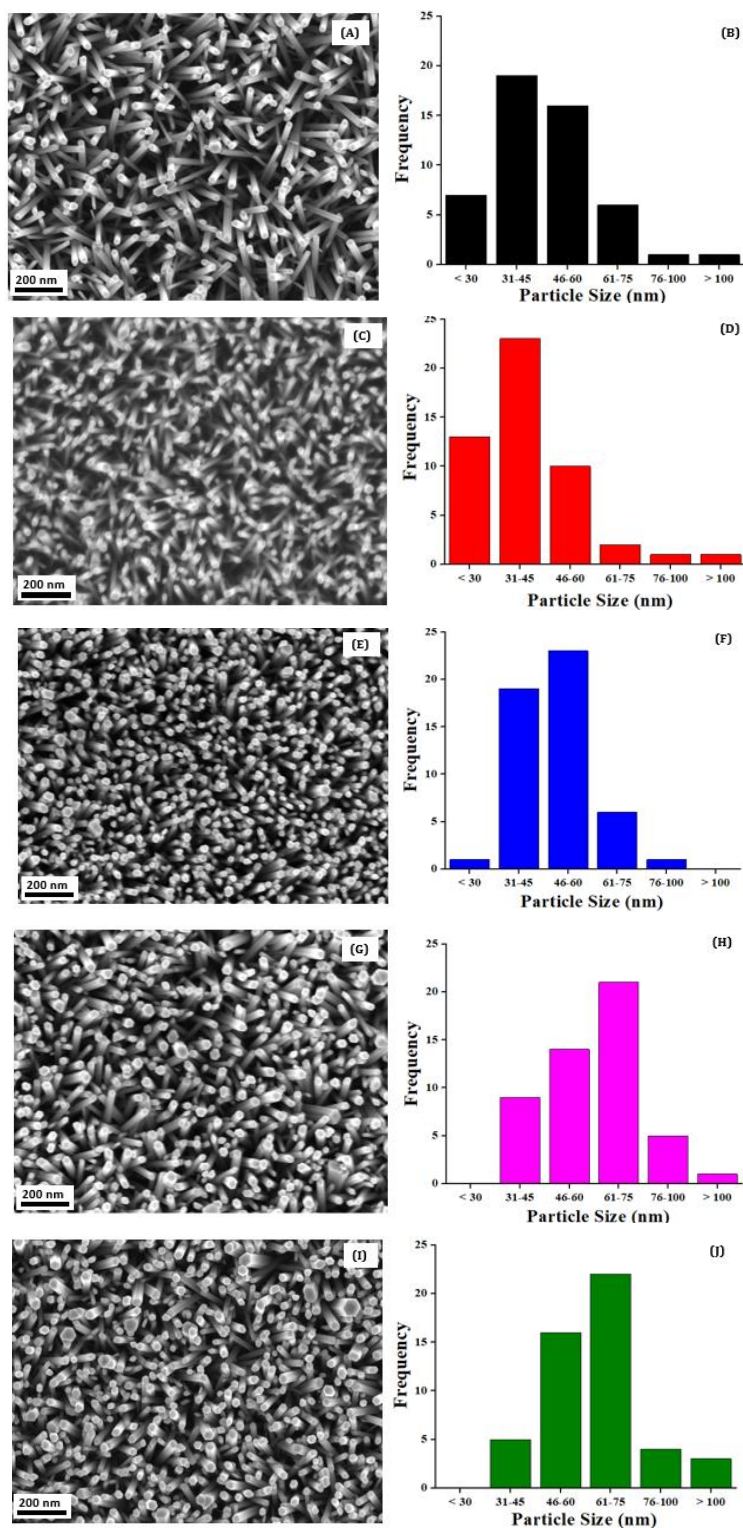

FIGURE 1. FESEM Images and particle size distribution of ZnO Pure (A,B), ZnO + Se 0.025 mL (C,D), ZnO + Se 0.05 mL (E,F), ZnO + Se 0.1 mL (G,H), and ZnO + Se 0.2 mL (I,J)

TABLE 1. Particle size distribution data of the sample ZnO pure and Se-ZnO

Sample	Nanorod diameter (nm)
ZnO Pure	46.89 ± 15.9
ZnO + Se 0.025 mL	38.78 ± 10.7
ZnO + Se 0.050 mL	48.68 ± 11.1
ZnO + Se 0.100 mL	60.72 ± 16.7
ZnO + Se 0.200 mL	64.68 ± 18.0

Based on Table 1, the addition of Se to ZnO affects the size of the nanorod diameter of the grown sample. ZnO+Se 0.025 mL and ZnO+Se 0.05 mL samples nanorods diameter are 38.78 ± 10.7 nm and 48.68 ± 11.1 nm, respectively. Table 1 and the histogram in Figure 1(d), 1(f) indicates ZnO+Se 0.025 mL and ZnO + Se 0.05 mL samples have the lowest standard deviation with more than 40% nanorod diameter in the range of 31-45 nm and 46-60 nm, respectively. It is clearly seen that Se doping decrease nanorods size as well as improve size distibution. Fortunately, doping that creates uniform nanorods mostly can enhance the optical and electrical properties of the ZnO nanostructure (Kim et al. 2014).

CRYSTAL STRUCTURE

The XRD pattern of pristine ZnO and Se-doped ZnO (Se-ZnO) nanorods are shown in Figure 2. There are five diffraction peaks detected at 2θ of 34.44°, 36.25°, 37.78°, 47.54°, and 51.63°. The 2θ of 34.44°, 36.25°, and 47.54° correspond to reflection plane of ZnO hkl plane of (002), (101), and (102). The other two peaks with asterisk (*) refer to FTO plane of (220) and (211). The diffraction peaks of both undoped and Se doped ZnO samples indicates the hexagonal wurtzite ZnO (JCPDS No. 01-070-8070) (Chen et al. 2017). The highest diffraction peak at (002) suggests the growth direction of the Se-ZnO nanorod along the c-axis which is perpendicular to the FTO surface. The similar results are also reported previously (Taha et al. 2019) for ZnO doped with 2% mol of Se.
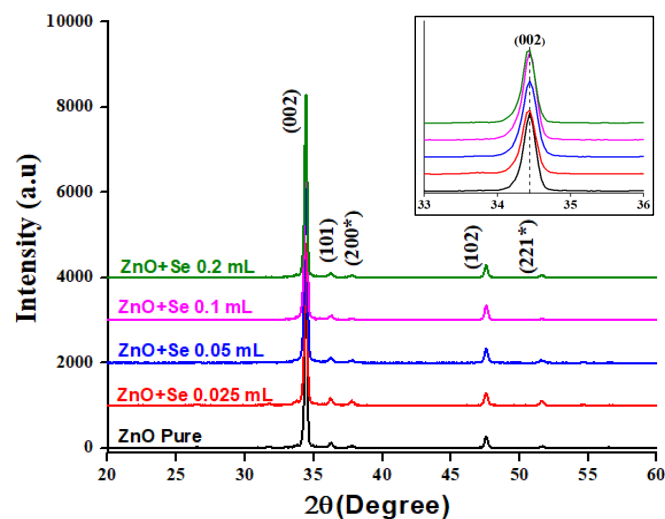

FIGURE 2. XRD patterns of ZnO pure and Se doped O. Inset is magnification of (002) peaks

The inset of Figure 2 displays the magnification of the (002) peaks of the undoped and Se doped ZnO nanorods. The peak posisiton of doped ZnO slightly shifted towards lower angles relative to that of undoped ZnO. It is indicating that the Se had succesfully penetrated into the ZnO lattice (Chen et al. 2017) and increased the lattice parameters (Wang et al. 2015). The crystal size (D) of the sample can be calculated by the Debye-Scherrer equation (Patterson 1939).

$$D = \frac{k\lambda}{\beta \cos\theta} \tag{1}$$

where $k, \lambda, \beta,$ and θ represent a constant equal to 0.90, the wavelength of the incident X-ray (1.5406 Å), full width at half maximum (FWHM) and peak position (in degree), respectively. Peak widening of FWHM is associated with reduced crystal size. Crystallite size were estimated from the strogest peak (002) data, and the lattice parameter were calculated from (101) and (002) peak, as shown in Table 2.

TABLE 2. Crystallite size and lattice constant values for the undoped and Se doped ZnO samples

Sample	2θ (°)	β_{FWHM} (°)	D (nm)	a=b (Å)	c (Å)	c/a
ZnO Pure	36.436	0.226	38.2	3.257	5.206	1.598
ZnO + Se 0.025 mL	36.434	0.245	35.3	3.257	5.214	1.601
ZnO + Se 0.05 mL	34.434	0.237	36.5	3.256	5.214	1.601
ZnO + Se 0.1 mL	34.435	0.208	41.6	3.257	5.206	1.598
ZnO + Se 0.2 mL	34.435	0.218	39.6	3.256	5.206	1.600

At lower Se doping concentration (ZnO+Se 0.025 mL and ZnO+Se 0.05 mL), the diffraction peak intensity is reduced along with FWHM broadening. Broadening of FWHM is associated with the reduction of crystallite size of ZnO due to the incorporation of Se into ZnO (Nenavathu et al. 2018). Decreasing of the Se-doped ZnO crystalline size might be due to te Se^{+4} (0.050 nm) displacement of Zn^{+2} (0.074) in the ZnO matrix (Taha et al. 2019). This reduction in crystallite size is similar to the previous report on the synthesis of Se-doped ZnO NPs (Taha et al. 2019). However, at the higher Se doping concentration (ZnO+Se 0.1 mL and ZnO+Se0.2 mL), the intensity of diffraction peaks are increased. This results is also consistent with Wang et al. (2019), which states that the peak intensity will increase with increasing doping volume up to 0.1%. ZnO + Se 0.1 mL sample has the largest crystal size or the highest crystallinity. The lattice

parameter slightly changes compared to the pure ZnO sample. Changes in lattice parameters were also observed in Se-doped ZnO films made using the thermomechanical method. The lattice parameter enlargment indicates that Se is integrated at both the interstitial and the O sites (Bae et al. 2004). The lattice parameters of ZnO+Se 0.05 mL and ZnO+Se 0.2 mL samples are slightly reduced $\pm$ 0.001 Å. The lattice c parameters of the ZnO+Se 0.025 mL and ZnO+Se 0.05 mL samples increased by 0.008 Å. Aspect ratio (c/a) of the pure ZnO and Se-ZnO samples are around 1.6. The aspect ratio values obtained are by the values obtained in the research conducted by Mustafa et al. (2018).

OPTICAL PROPERTIES

To analyze undoped and Se doped ZnO samples, with reflectance and absorbance measurements was performed
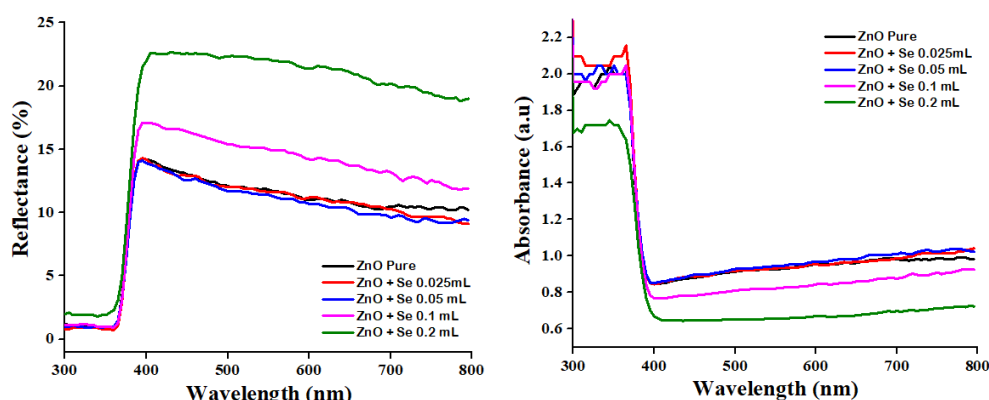

FIGURE 3. (a) Reflectance and (b) Absorbance spectra of ZnO and Se-doped ZnO samples with different dopant volume

using a UV-Vis spectrophotometer in the wavelength range of 300 - 800 nm. The UV-Vis reflectance and absorbance spectra of ZnO and Se-doped ZnO with different dopant volume are displayed in Figure 3(a) and 3(b).

The UV-Vis reflectance and absorbance spectra of ZnO and Se-doped ZnO with different dopant volume are displayed in Figure 3(a) and 3(b). For all samples, weak reflectance occurs in the range of 300-380 nm of wavelength, while the strong reflectance occurs in the range of 380-800 nm of wavelength. The highest strong reflectance spectrum belongs to the ZnO+Se 0.2 mL sample and the lowest strong reflectance belongs to ZnO+Se 0.05 mL sample. The strong reflectance peak shift toward the wavelength of visible light (red shift).

The absorption spectrum of the sample is shown in Figure 3(b). In the figure, it can be seen that the absorption intensity is inversly related to the reflectance intensity. The peak absorption of the ZnO nanorods occurs in the range of ultraviolet (UV) wavelength (Wang et al. 2019). The weak absorption occurs in the visible range which indicates the characteristics of the ZnO semiconductor (Sutanto et al. 2016). The increase in absorption intensity in the 300-380 wavelength range suggests more electrons from the sample being excited from a lower energy level to a higher energy level.

The band gap energy of each sample can also be determined from the reflectance and absorbance spectra. The band gap energy of the sample can be estimated using the Tauc plot equation,

$$\alpha h \upsilon^n = A(h\upsilon - Eg) \tag{2}$$

where α, h, v, A, and Eg represent the absorbance coefficient, Plank constant, frequency, proportionality constant, and band gap energy, respectively. Value n used for ZnO is 2, because ZnO is a direct band gap semiconductor. Band gap energy was determined by plotting the Tauc plot $(\alpha h\upsilon)^2$ vs vs $(h\upsilon)$. The band gap energy is obtained by extrapolating the linear curve to the x-axis $(h\upsilon)$. The Tauc plot of the undoped and Se doped ZnO sample were shown in Figure 4.
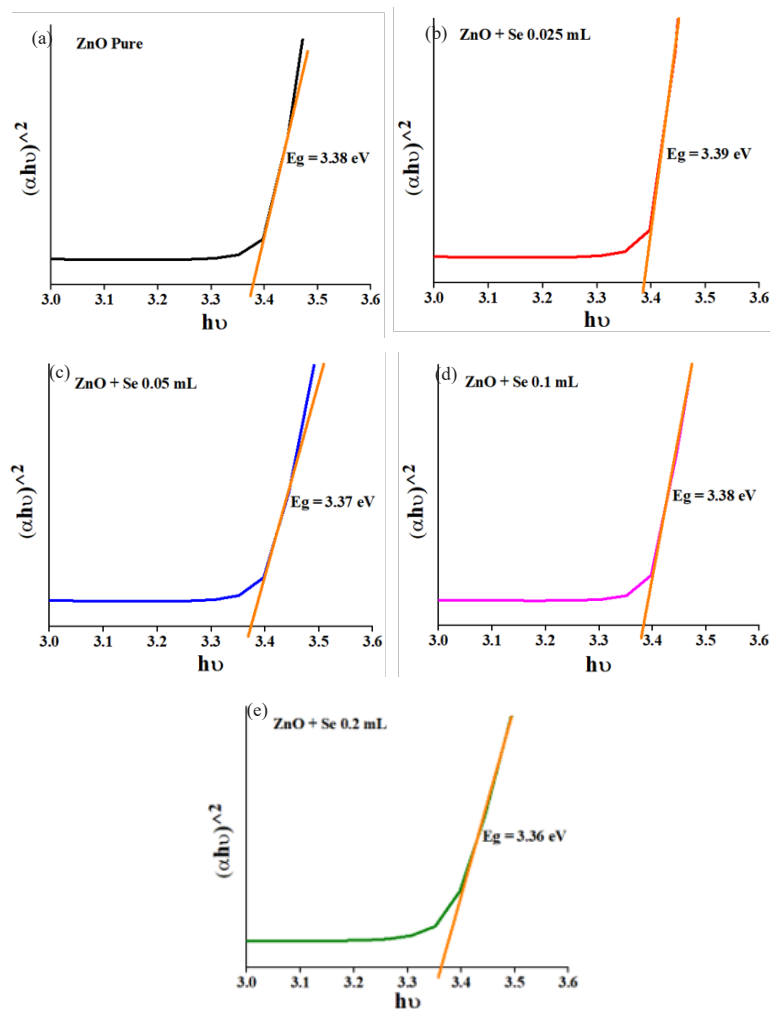

FIGURE 4. Tauc's plot of the undoped (a) and Se doped ZnO samples with different dopant volume (b) Se 0.025mL, (c) Se 0.05 mL, (d) Se 0.1 mL, and (e) Se 0.2 mL

According to Figure 4(a), band gap energy of pure ZnO nanorods is 3.38 eV. Low addition of dopant volume less than 0.2 mL has slightly changed the band gap energy ± 0.01eV. The lowest band gap energy is found in the sample with the addition of Se 0.2 mL (~3.36 eV). The doping effect in semiconductor nanoparticles normally change both valence band (VB) or conduction band (CB) energy level, causing the widening or narrowing of the band gap (Walsh et al. 2008). According to the Burstein-Moss theory, electrons donor in Se-doped ZnO occupy the bottom of the ZnO conduction band (Chen et al. 2017). A small decrease in the band gap energy in the ZnO+Se 0.2 mL sample indicates an additional energy bands from the doping element into the ZnO nanorods conduction band (Ashari et al. 2016). The band gap energy reduction of the Se-doped ZnO nanorods sample was also obtained in the study of Taha et al. (2019). The reduction of band gap energy indicates that more valence band electron experience transition to the conduction band (Duan et al. 2006). However, increase of band gap energy caused by ZnO doping with Se might be occured after Se/ZnO molar ratio of 1:1, as previously reported (Chen et al. 2017).

Figure 5 shows the photoluminescene spectra of doped and undoped ZnO nanorods. The peak emissions that occur in the sample are blue emission bands. This emission band is related to near band edge (NBE) caused by an oxygen vacancy (Kannappan & Dhanasekaran 2014).
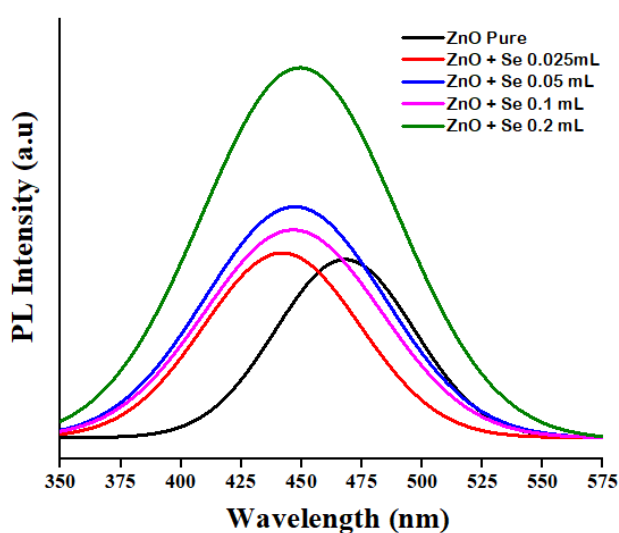

FIGURE 5. Photoluminescence spectra of ZnO pure and Se-ZnO

The peak of pure ZnO nanorods emission occurs at the wavelength of 470 nm. On the other hand, with the addition of the Se element into ZnO, the emission peak increases and shifts towards the greater energy. The raise in the intensity of the blue emission band attribute to an increase in the concentrations of Se atoms. This result was also obtained by Nenavathu et al. (2018) who doped 5% of Se to ZnO. The PL intensity of Se-doped ZnO nanoros is higher than pure ZnO, indicating that the recombination of electrons and photo-induced holes still occurs (Chen et al. 2017). The shift in peak NBE emissions that occured can be ascribed to the incorporation of dopants, which causes a change in the band gap energy value.

CONCLUSION

In summary, undoped and Se-doped ZnO nanoparticles have been synthesized by the seed-mediated hydrothermal method. FESEM images show the samples are nanorod shaped. XRD analysis showed that the average crystallite size of obtained ZnO in the ranges of 35 to 42 nm with average aspect ratio of 1.6. The optical properties of ZnO pure and Se-doped ZnO was evaluated by UV-Vis reflectance and absorbance spectra. The band gap energy shows no significant changes that occurred with value 3.38 eV. Besides, the PL spectrum shows that the recombination of electrons and photogeneration of holes still occurs.

REFERENCES

Abrar, I., Dee, C.F., Gebeshuber, I.C. & Majlis, B.Y. 2012. Growth and characterization of indium doped ZnO nanowires using vapor transport deposition method. *Advanced Materials Research* 364: 202-205.

Achouri, F., Corbel, S., Balan, L., Mozet, K., Girot, E., Medjahdi, G., Said, M.B., Ghrabi, A. & Schneider, R. 2016. Porous Mn-doped ZnO nanoparticles for enhanced solar and visible light photocatalysis. *Materials and Design* 101: 309-316.

Alexandrov, A., Zvaigzne, M., Lypenko, D., Nabiev, I. & Samokhvalov, P. 2020. Al-, Ga-, Mg-, or Li-doped zinc oxide nanoparticles as electron transport layers for quantum dot light-emitting diodes. *Scientific Reports* 10(1): 1-11.

Alshammari, A.S., Chi, L., Chen, X., Bagabas, A., Kramer, D., Alromaeh, A. & Jiang, Z. 2015. Visible-light photocatalysis on C-doped ZnO derived from polymer-assisted pyrolysis. *RSC Advances* 5(35): 27690-27698.

Ashari, F., Chyi, J.L.Y., Talib, Z.A., Yunus, W.W.W., Jian, L.Y. & Kee, L.H. 2016. Optical characterization of zinc selenide compound prepared through hydrothermal method. *Materials Science Forum* 846: 237-244.

Bae, S.Y., Seo, H.W. & Park, J. 2004. Vertically aligned sulfur-doped ZnO nanowires synthesized via chemical vapor deposition. *Journal of Physical Chemistry B* 108(17): 5206-5210.

Bangbai, C., Chongsri, K., Pecharapa, W. & Techitdeera, W. 2013. Effect of Al and N doping on structural and optical properties of sol-gel derives ZnO thin films. *Sains Malaysiana* 42(2): 239-246.

Chen, L.C., Tu, Y.J., Wang, Y.S., Kan, R.S. & Huang, C.M. 2008. Characterization and photoreactivity of N-, S-, and C-doped ZnO under UV and visible light illumination. *Journal of Photochemistry and Photobiology A: Chemistry* 199(2-3): 170-178.

Chen, Y., Wang, L., Wang, W. & Cao, M. 2017. Synthesis of Se-doped ZnO nanoplates with enhanced photoelectrochemical and photocatalytic properties. *Materials Chemistry and Physics* 199: 416-423.

Corral-Aguado, A., Martínez-Torres, P., Gomez-Ortiz, N., Pichardo-Molina, J., De la Rosa-García, S., Borjas-García, S.E. & Medina, A. 2016. Synthesis of Mg doped ZnO with hexagonal shape by hydrothermal method. *Microscopy and Microanalysis* 22(S3): 1882-1883.

Duan, L., Lin, B., Zhang, W., Zhong, S. & Fu, Z. 2006. Enhancement of ultraviolet emissions from ZnO films by Ag doping. *Applied Physics Letters* 88(23): 1-4.

Janotti, A. & Van De Walle, C.G. 2009. Fundamentals of zinc oxide as a semiconductor. *Reports on Progress in Physics* 72(12): 1-29.

Kannappan, P. & Dhanasekaran, R. 2014. Studies on structural and optical properties of ZnSe and ZnSSe single crystals grown by CVT method. *Journal of Crystal Growth* 401: 691-696.

Karim, S.S.A., Dee, C.F., Majlis, B.Y. & Mohamed, M.A. 2019. Recent progress on fabrication of zinc oxide nanorod-based field effect transistor biosensors. *Sains Malaysiana* 48(6): 1301-1310.

Kim, S., Park, H., Nam, G., Yoon, H., Kim, B., Ji, I., Kim, Y., Kim, I., Park, Y., Kang, D. & Leem, J.Y. 2014. Hydrothermally grown boron-doped ZnO nanorods for various applications: Structural, optical, and electrical properties. *Electronic Materials Letters* 10: 81-87.

Kumar, S.O., Soundeswaran, S. & Dhanasekaran, R. 2002. Thermodynamic calculations and growth of ZnSe single crystals by chemical vapor transport technique. *Crystal Growth and Design* 2(6): 585-589.

Luo, J., Wang, Y. & Zhang, Q. 2018. Progress in perovskite solar cells based on ZnO nanostructures. *Solar Energy* 163: 289-306.

Mustafa, M.M., Ahmed, H.A.M., Taha, K.K. & Mohammed, R. 2018. Synthesis and characterization of selenium doped zinc oxide (ZnO-Se) nanoparticles. *International Journal of Current Research* 10(9): 73644-73648.

Nenavathu, B.P., Sharma, A. & Dutta, R.K. 2018. Se doped ZnO nanoparticles with improved catalytic activity in degradation of Cholesterol. *Journal of Water and Environmental Technology* 3(4): 289-300.

Patterson, A.L. 1939. The Scherrer formula for X-ray particle size determination. *Physical Reviews* 56(10): 978-982.

Rahman, M.Y.A., Roza, L., Umar, A.A. & Salleh, M.M. 2016. Effect of dimethyl borate composition on the performance of boron doped ZnO dye-sensitized solar cell (DSSC). *Journal of Materials Science: Materials in Electronics* 27(3): 2228-2234.

Rong, P., Ren, S. & Yu, Q. 2019. Fabrications and applications of ZnO nanomaterials in flexible functional devices - A review. *Critical Reviews in Analytical Chemistry* 49(4): 336-349.

Singh, S.C. 2013. Zinc oxide nanostructures: Synthesis, characterizations and device applications. *Journal of Nanoengineering and Nanomanufacturing* 3(4): 283-310.

Sutanto, H., Wibowo, S., Nurhasanah, I., Hidayanto, E. & Hadiyanto, H. 2016. Ag doped ZnO thin films synthesized by spray coating technique for methylene blue photodegradation under UV irradiation. *International Journal of Chemical Engineering* 2016: 1-6.

Taha, K.K., Mustafa, M.M., Ahmed, H.A.M. & Talab, S. 2019. Selenium zinc oxide (Se/ZnO) nanoparticles: Synthesis, characterization, and photocatalytic activity. *Zeitschrift für Naturforschung A* 74(12): 1043-1056.

Tan, R., Zhang, Y.L., Yang, Y., Song, W., Xu, T.F. & Nie, Q. 2009. Pyroelectric properties of ZnO-based nanostructured polycrystalline ceramics. *International Symposium on Photoelectronic Detection and Imaging 2009: Material and Device Technology for Sensors*. doi.org/10.1117/12.836518.

Thangavel, R. & Chang, Y.C. 2012. Investigations on structural, optical and electrical properties of p-type ZnO nanorods using hydrothermal method. *Thin Solid Films* 520(7): 2589-2593.

Thu, T.V. & Maenosono, S. 2010. Synthesis of high-quality Al-doped ZnO nanoink. *Journal of Applied Physics* 107(1): 1-6.

Walsh, A., Da Silva, J.L.F. & Wei, S.H. 2008. Origins of band-gap renormalization in degenerately doped semiconductors. *Physical Review B* 78(7): 075211.

Wang, M., Ren, F., Zhou, J., Cai, G., Cai, L., Hu, Y., Wang, D., Liu, Y., Guo, L. & Shen, S. 2015. N doping to ZnO nanorods for photoelectrochemical water splitting under visible light: Engineered impurity distribution and terraced band structure. *Scientific Reports* 5: 1-13.

Wang, X., Huang, H., Liang, B., Liu, Z., Chen, D. & Shen, G. 2013. ZnS nanostructures: synthesis, properties, and applications. *Critical Reviews in Solid State and Materials Sciences* 38(1): 57-90.

Wang, Y., Zhong, M., Wang, W., Wang, Q., Wu, W. & Luo, X. 2019. Effects of ZnSe modification on the perovskite films and perovskite solar cells based on ZnO nanorod arrays. *Applied Surface Science* 495: 1-30.

Yilmaz, S., McGlynn, E., Bacaksiz, E., Cullen, J. & Chellappan, R.K. 2012. Structural, optical and magnetic properties of Ni-doped ZnO micro-rods grown by the spray pyrolysis method. *Chemical Physics Letters* 525-526: 72-76.

Zakaria, M.R., Johari, S., Ismail, M.H. & Hashim, U. 2017. Characterization of zinc oxide (ZnO) piezoelectric properties for surface acoustic wave (SAW) device. *International Conference on Applied Photonics and Electronics 2017 (InCAPE2017)*. Avillion Port Dickson, Malaysia. p. 01055.

Zhu, L. & Zeng, W. 2017. Room-temperature gas sensing of ZnO-based gas sensor: A review. *Sensors and Actuators A: Physical* 267: 242-261.

Ari Sulistyo Rini*, Yolanda Rati, Miranti Agustin & Yanuar Hamzah
Department of Physics
Faculty of Mathematics and Natural Science
Universitas Riau
Kampus Bina Widya
Jl. H.R Soebrantas Km 12.5, Simpang Baru
Pekanbaru, 28293
Indonesia

Akrajas Ali Umar
Institute of Microengineering and Nanoelectronics (IMEN)
Universiti Kebangsaan Malaysia
43600 UKM Bangi, Selangor Darul Ehsan
Malaysia

*Corresponding author; email: ari.sulistyo@lecturer.unri.ac.id